

# Early detection of biomolecular changes in disrupted porcine cartilage using polarized Raman spectroscopy

Natalie Sheng Jie Lim,<sup>a</sup> Zaribafzadeh Hamed,<sup>a</sup> Chen Hua Yeow,<sup>a</sup> Casey Chan,<sup>a,b</sup> and Zhiwei Huang<sup>a</sup>

<sup>a</sup>National University of Singapore, Faculty of Engineering, Department of Bioengineering, Optical Bioimaging Laboratory, Singapore 117576

<sup>b</sup>National University of Singapore, Yong Loo Lin School of Medicine, Department of Orthopaedic Surgery, Singapore 119074

**Abstract.** We evaluate the feasibility of applying polarized Raman spectroscopy in probing the early biochemical compositions and orientation changes in impacted porcine cartilage explants. We divide 100 fresh tibial cartilage explants into four groups: control (unimpacted) and 3 groups of single impact at 15, 20, and 25 MPa. Each group is examined for biochemical changes using Raman microscopy, cell viability changes using confocal fluorescence microscopy, and histological changes using the modified Mankin score. For the 15-MPa impact group, the modified Mankin score ( $p > 0.05$ ,  $n = 15$ ) and cell viability test ( $p > 0.05$ ,  $n = 5$ ) reveal no significant changes when compared to the control, but polarized Raman spectroscopy detects significant biochemical changes. A significant decrease in the parallel polarized intensity of the pyranose ring band at  $1126\text{ cm}^{-1}$  suggests a possible decrease in the glycoaminoglycan content in early cartilage damage (one-way analysis of variance with a *post hoc* Bonferroni test,  $p < 0.05$ ,  $n = 10$ ). For impacts greater than 15 MPa, cell viability and modified Mankin score are consistent with the changes in the observed polarized Raman signals. This suggests that the polarized Raman spectroscopy technique has potential for diagnosis and detection of early cartilage damage at the molecular level. © 2011 Society of Photo-Optical Instrumentation Engineers (SPIE). [DOI: 10.1117/1.3528006]

Keywords: cartilage; biomolecular changes; collagen; osteoarthritis; polarized Raman spectroscopy; Mankin score.

Paper 10457RR received Aug. 15, 2010; revised manuscript received Nov. 8, 2010; accepted for publication Nov. 10, 2010; published online Jan. 12, 2011.

## 1 Introduction

Early cartilage disruption occurs at a biomolecular level but often shows no abnormality in surface appearance or color.<sup>1</sup> It is characterized by the disruption of collagen fibers in the superficial and middle layers, loss of proteoglycans, and chondrocyte death.<sup>2,3</sup> However, such biomolecular changes cannot be accurately detected by current clinical techniques such as conventional radiography and computed tomography. Even magnetic resonance imaging (MRI), which is believed to be a promising noninvasive method for early detection,<sup>4</sup> still encounters artifacts and low resolution. This hinders the monitoring of the degeneration of cartilage at microstructural level.<sup>5</sup> The underlying physical effects of MRI are too weak to detect changes at molecular resolution.<sup>6</sup>

Raman spectroscopy is an inelastic scattering process capable of providing information about biochemical and biomolecular structures and conformations of samples. It was shown to be a promising means in characterizing biomolecular changes associated with diseased transformation.<sup>7</sup> Unlike the complementary vibration technique, infrared (IR) spectroscopy, near-infrared (NIR) Raman spectroscopy encounters less interference from water in tissue, eliminating the undesirable necessity to process or dehydrate the samples before determining the biochemical spectra.<sup>8</sup> This makes the NIR Raman spectroscopy technique especially advantageous for the characterization of

biomolecular changes in live cartilage tissues comprising up to 70% water.<sup>9</sup> Recently, Raman spectroscopy has been comprehensively investigated for studying the structures of proteoglycans and glycosaminoglycans<sup>10</sup> (GAG), biomolecular changes in strained collagen tendon fibers,<sup>11</sup> changes in collagen tendon fiber orientation,<sup>12</sup> defective ocular collagen fibers,<sup>13</sup> and also the subchondral bone of transgenic mouse with early onset of osteoarthritis.<sup>14</sup> The Raman spectra of these specific biocomponents provide a framework for the analysis of cartilage. However, so far, there is a lack of knowledge about the polarization effects of the Raman spectra of full depth cartilage. Since Raman scattered light is dependent on both the composition and structure of tissue,<sup>7</sup> the polarization of scattered Raman light relative to the input laser polarization may provide valuable information on the biomolecular orientation changes of tissue and help distinguish preferentially oriented chemical bonds from randomly oriented chemical bonds within the tissue.<sup>15</sup> As impact stress on the articular cartilage surface greater than 20 MPa incurred from car accidents or even landing impacts from sports has been shown to induce moderate to late stages of articular cartilage damage<sup>16–18</sup> (Mankin scores greater than 6.3), possible disruptions in the preferential fibril orientation of collagen fibers<sup>9,19,20</sup> and GAG rod orientations<sup>21</sup> may be detected using polarized Raman spectroscopy. In this paper, we evaluate the feasibility of applying the polarized Raman spectroscopy technique to probe biomolecular changes in disrupted cartilage even prior to visible histological change. The fresh porcine tibial osteochondral explants were impacted at 15, 20, and 25 MPa, respectively. The impacted

Address all correspondence to: Zhiwei Huang, Optical Bioimaging Laboratory, Department of Bioengineering, Faculty of Engineering, National University of Singapore, 9 Engineering Drive 1, Singapore 117576. Tel: +65-6516-8856; Fax: +65-6872-3069; E-mail: biehw@nus.edu.sg

explants were incubated in cell culture medium for a week and thereafter evaluated for biochemical changes using both nonpolarized and polarized Raman spectroscopy. The polarized tissue Raman spectra were also correlated with histological changes and cell viability.

## 2 Material and Methods

### 2.1 Specimen Preparation—Day 0

Fresh hind legs were obtained from 2- to 5-month-old pigs, weighing about 40 kg from the Primary Industries abattoir in Singapore. Each hind leg was dissected above the knee joint within 3 h of slaughter. Using a trephine, 100 full-depth cartilage explants of 4 mm in diameter and 2.5 mm in depth were extracted from the menisci-covered tibial region.<sup>16</sup> These explants were randomly divided into four equal groups: the control (unimpacted healthy cartilage) and three groups that were subjected to unconfined single impact loads of 15, 20, and 25 MPa (Refs. 16 to 18). All explants were immediately immersed in isotonic Dulbecco modified Eagle medium (DMEM, 280 mOsm, pH 7.4) (Gibco, Basel, Switzerland) supplemented with 1-g/L L-glutamine, 10-mg/mL streptomycin sulfate, 10,000-units/mL penicillin G sodium, and 10% (v/v) fetal bovine serum<sup>19</sup> (Sigma-Aldrich, St. Louis, Missouri). They were incubated at 37°C and 5% CO<sub>2</sub> in a humidity-controlled incubator for up to 7 days. The cell culture medium was changed every 3 days.

### 2.2 Single Impact-Unconfined Compression—Day 0

Three groups of explants were subjected to a single impact-unconfined compression. A stainless steel 10-mm-diam compression plate and a dental cement pot (base-liquid and powder, Dentsply, Tianjin, China) was attached to the single column testing system (Instron, model 3345, Norwood, Massachusetts). Each moist explant from the impact group was placed on a sterile dental cement pot directly beneath the compression plate. A compression preload of 10 N was applied to ensure that the entire surface of the cartilage was in close contact with the compression plate. The impact groups were subjected to the corresponding peak stresses (15, 20, or 25 MPa) at a displacement rate of 2 mm/s using a uniaxial  $5 \times 10^3$  N load cell. After each impact, the explant was removed from the dental cement pot, immersed in fresh cell culture medium, and incubated. Control and impacted explants were randomly selected for cell viability assessment, histology, and Raman spectroscopy on day 7.

### 2.3 Cell Viability Test—Day 7

On day 7, explants ( $n = 5$  for each impact group) were removed from the cell culture medium and incubated for 30 min in 2 ml of medium of 0.1% fluorescein diacetate, and 0.05% propidium iodide (Sigma-Aldrich, St. Louis, Missouri). A confocal fluorescence microscope (Fluoview FV300; Olympus) with an excitation wavelength of 488 nm was used to image the cells on the cartilage surface, called chondrocytes. To visualize live cells, a narrow-bandpass filter centered at 550 nm (green) with an FWHM of 20 nm was used. To visualize dead cells, a narrow-bandpass filter centered at 650 nm (red) with an FWHM of 20 nm was used. A 20× objective lens was used to obtain images of the center of each explant. Pixel area fractions of viable and non-

viable cells were calculated using Image J (Version 1.4; NIH, Bethesda, Maryland). From these images, the percentage cell viability, given as  $P_L / (P_L + P_D)$ , where  $P_L$  is the number of green pixels representing live cells, and  $P_D$  is the number of red pixels representing dead cells, was calculated. Their values were normalized and thereafter compared between the control and each impacted group.

### 2.4 Histology Protocol—Day 7

On day 7, explants ( $n = 15$  for each impact group) were fixed in 10% buffered formalin on a shaker for 2 weeks and then decalcified in 30% formic acid for another 2 weeks. Thereafter, the explants were dehydrated and cleared in ethanol and toluene for 16 h. The explants were then embedded in paraffin blocks and 8- $\mu$ m cartilage slices were obtained using a microtome (RM2255, Leica Microsystems, Nussloch, Germany). Next, the sections were deparaffinized and stained using hematoxylin and eosin and Safranin-O/Fast Green to visualize the osteochondral structure, cell distribution, and proteoglycan or GAG contents. The histological appearance of the cartilage was finally evaluated by five independently trained investigators blinded against the control and impact groups to eliminate any bias. A modified Mankin scoring system was employed to grade the extent of cartilage disruption<sup>22-24</sup> (Table 1).

### 2.5 Raman Spectrometry Test—Day 7

We compared linearly polarized (i.e., perpendicular and parallel polarized) Raman spectra of porcine explants ( $n = 10$  for control and 15-MPa impact groups;  $n = 5$  for 20- and 25-MPa impact groups) with the nonpolarized Raman spectra of the same explant on coverslips (vfm coverslips, CellPath Ltd., United Kingdom) using a confocal Raman spectrometer system (inVia, Renishaw, United Kingdom) coupled with a microscope (DMI 5000M, Leica) in a backscattering geometry.<sup>25</sup> The parallel- or perpendicular-polarized micro-Raman measurements were performed by changing the direction of a linear polarizer (analyzer) placed in front of the CCD detector to be parallel or perpendicular with respect to the polarization direction of the linear polarizer placed in front of the 785-nm laser. The 785-nm laser beam (maximum output of 100 mW, Renishaw, United Kingdom) was focused onto explant with a beam size of  $\sim 1 \mu$ m via a microscope objective [40×, numerical aperture (NA) 0.9, Leica, Germany]. The tissue Raman spectra were detected by a NIR-enhanced CCD detector (Peltier cooled at  $-70^\circ\text{C}$ , Renishaw, United Kingdom) through a Czerny-Turner-type spectrograph ( $f = 250$  mm) equipped with a holographic grating (1800 gr/mm). The spectral resolution of the micro-Raman system is  $\sim 4 \text{ cm}^{-1}$ . The nonpolarized and polarized (i.e., parallel and perpendicular) micro-Raman spectra can be acquired in tandem on the same samples by our confocal micro-Raman system. Each Raman spectra was collected with an integration time of 5 s and a 785-nm laser illumination power of  $\sim 1$  mW on the samples.

### 2.6 Raman Data Processing

Each raw Raman spectrum was smoothed using the third-order Savitzky-Golay smoothing filter, and the fifth-order

**Table 1** Modified Mankin scores grading system (Refs. 22–24).

Section 1: Structure	Grade
Normal structure	0
Surface irregularities: with no clefts	1
Surface irregularities: clefts limited to superficial zone	2
Clefts into the middle (transitional zone)	3
Clefts into the deep (radial) zone	4
Clefts to the calcified zone (tidemark)	5
Complete disorganization	6
Section 2: Safranin-O-Staining	Grade
Normal	0
Slight reduction	1
Moderate reduction	2
Severe reduction	3
No dye noted	4
Section 3: Tidemark Integrity	Grade
Intact	0
Disrupted	1
Total Scores	Min 0
	Max 11

polynomial<sup>26–28</sup> was found to be optimal for fitting the autofluorescence background in the noise-smoothed spectrum. This polynomial was subtracted from the smoothed raw spectrum to yield the tissue Raman spectrum alone.<sup>27</sup> The multiple-component model was used to deconvolute selected Raman bands. To facilitate a computer fit to the data, the component Raman spectral intensity  $I(x)$  was assumed to be Gaussian<sup>29</sup>:

$$I(x) = \sum_{i=1}^n H_i \exp \left[ -\frac{2(x - w_i)^2}{\Delta w_i^2} \right],$$

where

$$H_i = \frac{A_i}{\Delta W_i \sqrt{\pi/2}},$$

where  $H_i$  is the height of the respective Gaussian spectra,  $A_i$  is the total area under the curve from the baseline,  $W_i$  represents the center of the peak at which the Raman intensities reach maximum values for the two component spectra, and  $\Delta W_i$  is approximately 0.849 times the width of the peak at half height.<sup>29</sup> Results from the curve fit yielded an  $R^2$  value greater than 0.95 and no negative peaks were present. The proline ( $856 \text{ cm}^{-1}$ ); hydroxyproline ( $875 \text{ cm}^{-1}$ ) band area ratios, pyranose ring band intensity ( $1126 \text{ cm}^{-1}$ ), and the full width at half maximum

(FWHM) of the amide I band ( $1665 \text{ cm}^{-1}$ ) were calculated from the respective Gaussian spectra fitted.

## 2.7 Statistical Analysis

A Mann-Whitney test was performed to compare the modified Mankin score from each impact group against the control group. In addition, a one-way analysis of variance (ANOVA) was performed followed by *post hoc* Bonferroni tests for comparison of modified Mankin scores, normalized cell viability scores and biochemical changes (e.g., pyranose intensity  $1126 \text{ cm}^{-1}$ , proline to hydroxyproline band areas ratio  $856 \text{ cm}^{-1}/875 \text{ cm}^{-1}$ , amide III band's red shift and FWHM of amide I band  $1664 \text{ cm}^{-1}$ ). Differences were considered significant at the  $p < 0.05$  level. An unpaired two-sided Student's  $t$  test was also used to compare changes between the FWHM of the parallel polarized amide I band and the FWHM of the perpendicular polarized amide I band within each impact and control group. Again, differences were considered significant at  $p < 0.05$ . To separate biochemical changes of impacted cartilage explants from control explants, the decision lines were selected using user-defined separate functions to obtain the optimal diagnostic specificity and sensitivity. The specificity was measured as the number of explants correctly identified as the normal unimpacted cartilage, while the sensitivity was measured as the number explants correctly identified as impacted cartilage.

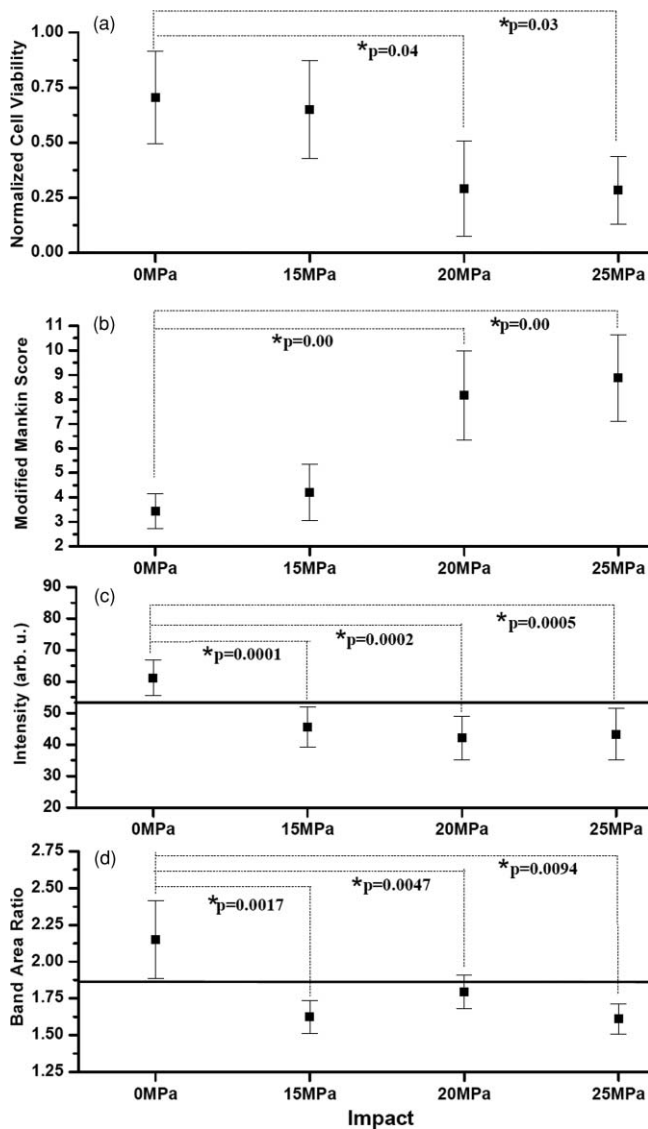
## 3 Results

### 3.1 Cell Viability

Figures 1(a) and 2 show the cell viability results for the control and impact groups. No significant cell death ( $p > 0.05$ , one-way ANOVA and *post hoc* Bonferroni test) was noted for the 15-MPa impact group ( $n = 5$ ) when compared to the control ( $n = 5$ ). However, significant chondrocytes death ( $p < 0.05$ , one-way ANOVA and *post hoc* Bonferroni test) was noted for the 20- ( $n = 5$ ) and 25-MPa ( $n = 5$ ) impact groups. These results are consistent with previous chondrocytes viability findings<sup>18</sup> that the threshold for cell death was between 15 and 20 MPa.

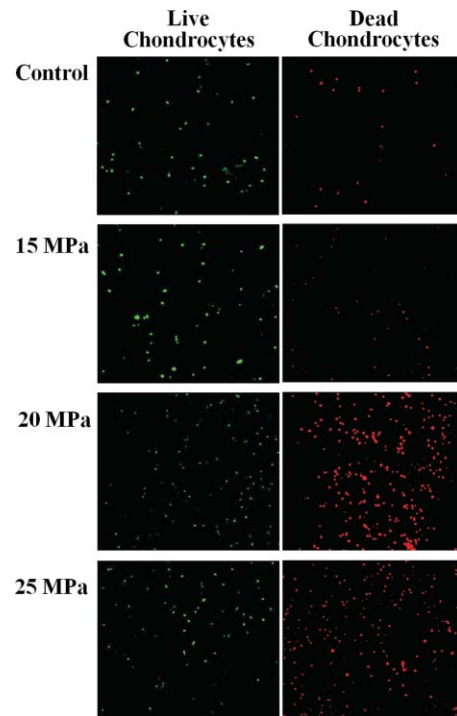
### 3.2 Histological Findings

Figure 3 shows the example of the histological slides for the 15-MPa impacted explants, revealing surface irregularities with fibrillation and small clefts limited to the superficial zone. Slight reductions of PG staining were also observed but no tidemark (boundary between calcified and uncalcified cartilage) disruptions were found. The mean modified Mankin score for the 15-MPa impacted explants was  $4.48 \pm 1.57$  points [Fig. 1(b)]. This score is classified as a mild osteoarthritic stage, grade I.<sup>24</sup> Statistically, this score is not significantly higher ( $p > 0.05$ ) than modified Mankin score for the control group,  $3.64 \pm 1.02$  points ( $n = 15$ ). Hence, the modified Mankin score revealed no substantial structural changes between the control and the 15-MPa impact group. On the other hand, histological results for the 20- and 25-MPa impact groups (Fig. 3) revealed extended clefts from the superficial to the calcified zone. In these high-impact groups, tidemarks were disrupted and severe reduction in PG staining in deep regions was noted. Some explants were also found to have a complete disorganization of structure. The



**Fig. 1** (a) Comparison of normalized cell viability profile among the control ( $n = 5$ ) and impacted cartilage explants ( $n = 5$  for each group); (b) comparison of modified Mankin score profile of control ( $n = 15$ ) and impacted cartilage explants ( $n = 15$  for each group); (c) comparison of mean parallel polarized Raman intensity at  $1126\text{ cm}^{-1}$  among the control ( $n = 10$ ) and impacted 15- ( $n = 10$ ), 20- ( $n = 5$ ), and 25-MPa ( $n = 5$ ) cartilage explants, where the decision line ( $I_{1126} = 53$ ) yields a sensitivity of 90% and specificity of 90% to separate the control from the impact groups; and (d) comparison of the Raman band area ratio of proline ( $856\text{ cm}^{-1}$ ) to hydroxyproline ( $875\text{ cm}^{-1}$ ) from the parallel polarized Raman spectra among control and impacted cartilage explants, where the decision line ( $I_{856}/I_{877} = 1.85$ ) yields a sensitivity of 88% and specificity of 95% to separate the control from the impact groups. Note that the symbol \* denotes statistically significant difference detected between the impact group and the control group, where  $p < 0.05$ . The y axis error bars indicate  $\pm 1$  standard deviation (SD).

20- and 25-MPa impacted groups explants were graded with mean modified Mankin scores of  $8.16 \pm 1.83$  and  $8.42 \pm 2.34$  points ( $n = 15$ ), respectively [Fig. 1(b)]. These scores were classified as grade 4, a severe osteoarthritic stage,<sup>24</sup> which is significantly higher ( $p < 0.05$ ) than the control group. Hence, the modified Mankin score revealed significant structural changes in the 20- and 25-MPa impact groups.



**Fig. 2** Confocal images of the cartilage surfaces of control and impacted groups after 7 days. Green colors (pixels) in the first column represent live cells; red colors (pixels) in the second column represent dead cells [see Fig. 1(a) for normalized cell viability profiles]. (Color online only.)

### 3.3 Raman Spectroscopy Results for Cartilage

Multiple Raman spectra were measured from the control ( $n = 10$ ), 15- ( $n = 10$ ), 20- ( $n = 5$ ), and 25-MPa ( $n = 5$ ) impact groups, respectively. A maximum of four spectra on the same cartilage explants were obtained at various locations to reduce the chances of overheating,<sup>30</sup> and serious disturbances of the cellular structure. All cartilage explants were also kept moist with physiological saline solution during Raman measurements. Figure 4 shows the mean nonpolarized and polarized (parallel and perpendicular) Raman spectra of all impact and control groups, exhibiting similar Raman spectral shapes and primary bands positions. Raman peaks were observed at the following locations:  $856, 875, 940, 1003, 1042, 1126, 1160, 1207, 1265\text{--}1279, 1450, 1560,$  and  $1660\text{ cm}^{-1}$ . Table 2 outlines the tentative biochemical assignments of respective Raman peaks observed in porcine cartilage.<sup>10,13,14</sup> Exceptions were noted in the parallel polarized Raman band at  $957$  and  $1063\text{ cm}^{-1}$  (Fig. 5), where the phosphate shoulder peak at  $957\text{ cm}^{-1}$  was observed only in the impact groups but not in the control group, while the sulphate shoulder peak at  $1063\text{ cm}^{-1}$  was observed only in 15-MPa impact group. On the other hand, the mean perpendicular polarized Raman spectra [Fig. 4(c)] revealed a significant overlapping of Raman bands between  $800$  and  $1200\text{ cm}^{-1}$ . Compared to the parallel polarized Raman spectra [Fig. 4(b)], Raman bands at  $856, 875, 940, 957,$  and  $1560\text{ cm}^{-1}$  were not detected in the perpendicular polarized Raman spectra [Fig. 4(c)]. The perpendicular polarized Raman intensities for Raman bands at  $1003$  and  $1042\text{ cm}^{-1}$  [arrows in Fig. 4(c)] were found to be notably reduced by 3 to 4 times relative to the parallel polarized Raman

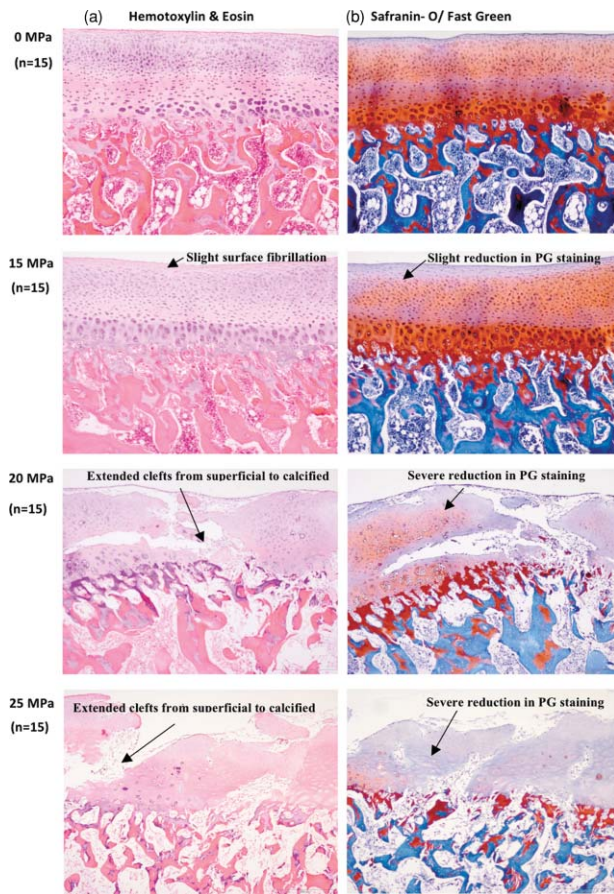


**Fig. 3** Histology slides of the sectioned cartilage explants stained using: (a) hemotoxylin and eosin and (b) Safranin-O/Fast Green. Slight reduction in proteoglycan (PG) staining with no matrix disruptions at 15-MPa impacted explants. Obvious reductions in proteoglycans staining and matrix disruptions are observed in 20- and 25-MPa impacted explants.

intensity [arrows in Fig. 4(b)]. This indicates that the Raman bands at  $1003$  and  $1042\text{ cm}^{-1}$  exhibit parallel dichroism in cartilage tissue.

### 3.4 Pyranose Ring Raman Band

For the pyranose ring Raman band at  $1126\text{ cm}^{-1}$  (arrow in Fig. 5), its mean parallel polarized Raman intensity was observed to have a significant decrease for all impact groups [Fig. 1(c)]. Note that the Raman intensity measurements were found to be quite consistent (of less than 5% variations in Raman intensities among different locations on the cartilages) for each group. Significant differences ( $p < 0.0005$ ) were obtained between the control and impact groups. The mean parallel polarized pyranose intensity of the control group can be separated from all impact groups with a 90% sensitivity and 90% specificity (when a decision line  $I_{1126} = 53$  is selected) [Fig. 1(c)]. In contrast, no decision line could be made to separate the control group from impact groups due to the insignificant modified Mankin scores between the control and 15-MPa impact groups [Fig. 1(b)]. For the mean nonpolarized pyranose intensity at  $1126\text{ cm}^{-1}$ , no statistical difference was found between the control and each impact group ( $p > 0.05$ ) [Fig. 6(a)].

### 3.5 Raman Band Area Ratio of Proline to Hydroxyproline

Figure 1(d) shows the mean Raman band area ratio values of proline ( $856\text{ cm}^{-1}$ ) to hydroxyproline ( $875\text{ cm}^{-1}$ ) in the parallel polarized spectra, illustrating the significant decrease ( $p < 0.05$ ) for all impact groups. In contrast to the modified Mankin scores [Fig. 1(d)], where no decision lines could be made, a separate line ( $I_{856}/I_{875} = 1.85$ ) can be determined to differentiate the mean proline:hydroxyproline band area ratios of the control from all the impact groups with a 95% sensitivity and 88% specificity. For the mean nonpolarized Raman spectra for proline: hydroxyproline band area ratios [Fig. 6(b)], there is no statistical difference between the control and the impact groups ( $p > 0.05$ ).

### 3.6 Amide III and Amide I Bands

As summarized in Table 3, a significant Raman shift of amide III peak position was noted in both the mean nonpolarized and parallel polarized Raman spectra. However, in the mean perpendicular polarized Raman spectra, the amide III Raman band appears to be doublet peaks at  $1264$  and  $1274\text{ cm}^{-1}$  for all the impact groups band, as compared to the singlet peak at  $1268\text{ cm}^{-1}$  for the control group (Fig. 7). For the amide I band at  $1664\text{ cm}^{-1}$ , its FWHM for each impact group was significantly narrower ( $p < 0.05$ , unpaired two-sided Student's  $t$  test) in the parallel polarized spectra [double arrows in Fig. 4(b)] compared to the perpendicular polarized spectra Fig. 4(c)]. Note that the mean amide I FWHM values of Raman spectra for the control group were  $60 \pm 11$  ( $n = 10$ ), and  $107 \pm 13$  ( $n = 10$ ), respectively, in the parallel and perpendicular polarized spectra. For the 15-MPa group, the mean amide I FWHM values were  $61 \pm 13$  ( $n = 10$ ) and  $107 \pm 20$  ( $n = 10$ ) in the parallel and perpendicular polarized spectra, respectively. For the 20-MPa impact group, the mean amide I FWHM values were  $65 \pm 10$  ( $n = 5$ ) and  $96 \pm 15$  ( $n = 5$ ) in the parallel polarized and perpendicular spectra, respectively. For the 25-MPa impact group, the mean amide I FWHM values were  $63 \pm 10$  ( $n = 5$ ) and  $113 \pm 8$  ( $n = 5$ ) in the parallel and perpendicular polarized Raman spectra, respectively.

## 4 Discussion

Our histology and cell viability results revealed that 7 days after impact, the cartilage explants in the 15-MPa impact group showed minimal damage while the cartilage explants in the 20- and 25-MPa impact groups exhibited severe damage. Similar results have been observed in other impact models.<sup>16,31-33</sup> In contrast to the lack of evidence of histological changes using conventional modified Mankin score for the 15-MPa impacted cartilage, in this paper, a wide spectrum of biomolecular changes associated with cartilage damage can be observed early using the polarized Raman spectroscopy.

The parallel polarized Raman spectra of porcine cartilage [Fig. 4(b)] show similar Raman spectral shapes and band positions to the rabbit nasal septa cartilage of rabbit,<sup>30</sup> except for the Raman band  $957\text{ cm}^{-1}$  associated with phosphate in the subchondral bone which was not reported. In our study, the phosphate Raman band ( $957\text{ cm}^{-1}$ ) in the parallel polarized

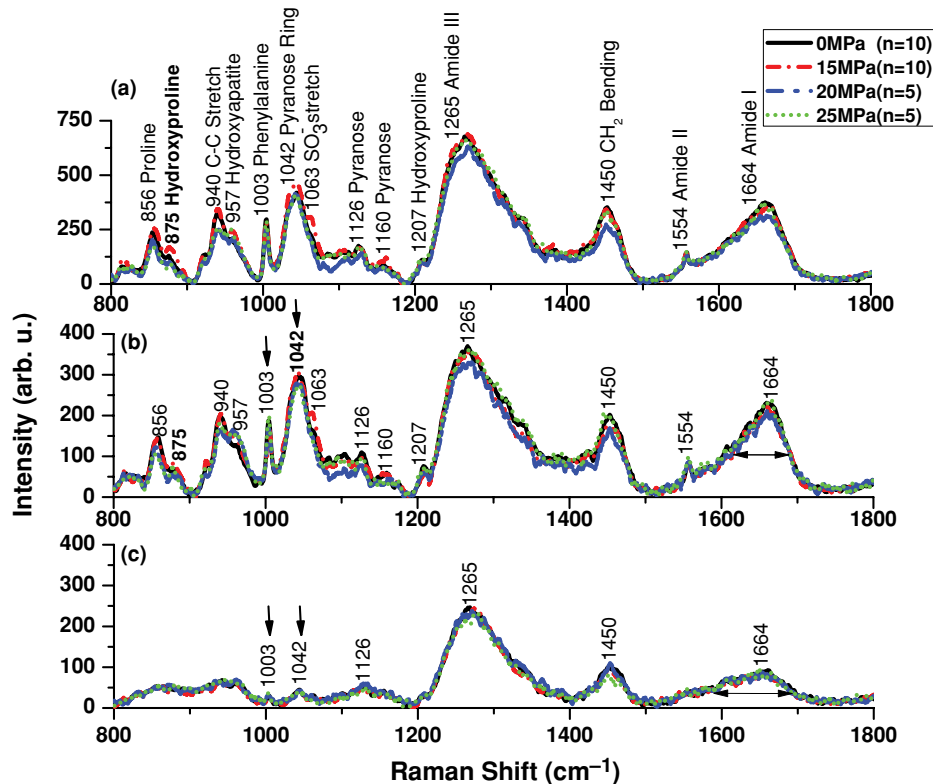


**Fig. 4** Comparison of Raman spectra among control and impacted porcine cartilage explants at 15, 20, and 25 MPa, respectively, obtained a week after impact: (a) mean nonpolarized Raman spectra, (b) mean parallel polarized Raman spectra, and (c) mean perpendicular-polarized Raman spectra. A single-headed arrow indicates the band where the parallel dichroism is observed, while the double-headed arrow indicates the FWHM of amide I raman band.

Raman spectra becomes visible after the porcine explants were impacted. This may be due to a decrease in the thickness of cartilage tissue after impact, resulting in a better detection of Raman signals emitted from deeper layers of the cartilage. However, the Raman signals at  $961\text{ cm}^{-1}$  ( $\nu_1$  phosphate marker) and  $1070\text{ cm}^{-1}$  (carbonate marker) associated with the subchondral layer<sup>14,15,34</sup> were not detected in all our Raman spectra. It was also reported that the phosphate contribution in the Raman spectra of subchondral bone was  $\sim 5$  to 7 times stronger than all the other contributions (e.g., the distinct amide III group associated with collagen<sup>15,34</sup>) from the bone. However, in our Raman spectra for impacted explants (Fig. 4), the relative intensity of the phosphate peak was noted to be  $\sim 0.3$  times the height of the amide III band. The weak phosphate signal observed indicates that the contributions from other biocomponents of the bone appear to be not dominant in cartilage Raman spectra. The contributions from cartilage continue to dominate the Raman spectra even after impact. The mean parallel polarized band area ratio of proline:hydroxyproline was found to decrease in all impact groups [Fig. 1(d)]. Proline and hydroxyproline are key components of collagen in the articular cartilage and play an essential role in the stability of the collagen helix.<sup>35</sup> Changes in the proline:hydroxyproline ratio suggest that the collagen helix stability may have been affected after impact.<sup>36,37</sup> In mildly disrupted cartilage, elevated rates of proline to hydroxyproline conversion by chondrocytes have been previously documented as a response to increase collagen synthesis.<sup>38</sup> Moreover in severely disrupted cartilage, it was previously reported that significant

chondrocytes death leads to a decrease in proline uptake.<sup>39</sup> Consequently, this may have also resulted in a decrease in band area ratio. Our current data, however, may not definitely discriminate among the stability of the collagen fibres in the superficial, middle, or deep cartilage layers due to a mixture of signals collected from the various layers.<sup>19,20</sup> Nevertheless, our results suggest that polarized Raman spectroscopy can detect a general loss of the collagen network integrity prior to significant chondrocyte death for the 15-MPa impact group. Meanwhile, to better understand the relationships between the cartilage-related morphologic/biochemical changes and the tissue Raman spectra for further improving tissue diagnosis and classification, confocal Raman microspectroscopy should be explored on the tissue *in vivo* or *in vitro*, by measuring the complete Raman spectra of specific tissue microstructures, or alternatively by mapping the distribution of some specific Raman peaks or principal components within a tissue, or even mapping the biochemical distributions at different tissue depths for association with cartilage damage. The work in these areas warrants further investigation.

We also observed a narrower FWHM of amide I band in the parallel polarized Raman spectra compared to the perpendicular polarized Raman spectra for all control and impact groups [double arrows in Figs. 4(b) and 4(c)]. This may indicate a less disperse distribution of dominant peptide carbonyl stretching in the parallel polarized direction. However, no significant changes in the FWHM of the amide I band were noted after impact for both the parallel and perpendicular polarized groups. No distinct parallel or perpendicular dichroism was observed either in all

**Table 2** Raman peak positions and tentative assignments of major vibrational bands observed in normal and impacted articular cartilage explants using polarized Raman spectroscopy (Refs. 10, 13, and 14).

Peak Position (cm <sup>-1</sup> )	Polarization Conditions			Assignments
	Non	Parallel	Perpendicular	
856	✓	✓	Broad Raman band between 860 and 880	(C—C) stretch, proline ring
875	✓	✓		(C—C) stretch, hydroxyproline ring
940	✓	✓	Broad Raman band between 940 and 959	(C—C) deformation, aggrecan/ (C—O—C) stretch, GAG
957*	✓	✓		PO <sub>4</sub> <sup>3-</sup> stretch; hydroxyapatite
1003	✓	✓	✓	(C—C) symmetric ring stretch; phenylalanine
1042	✓	✓	✓	Pyranose ring
1063	✓	✓		SO <sub>3</sub> <sup>-</sup> symmetric stretch; GAG
1126	✓	✓	✓	Pyranose ring
1160	✓	✓		Pyranose ring
1207	✓	✓		(C—C <sub>6</sub> H <sub>5</sub> ) stretch; phenylalanine tryptophan, hydroxyproline, tyrosine
1265–1279	✓	✓	✓	(C—N) stretch alpha-helix; amide III
1450	✓	✓	✓	(C—H) bend; protein CH <sub>2</sub> ,CH <sub>3</sub> scissor
1560	✓	✓		Amide II
1660	✓	✓	✓	(C = O) stretch alpha-helix; Amide I

✓: Peak present in Raman spectra; \* Peak only appears in impact groups.

amide bands. This may be attributed to the mixture of signals collected from the different arrangement of cartilage layers. It is known that in the superficial layer, collagen fibers are oriented parallel to the articular surface.<sup>9,19,20</sup> Thus, they have the lowest compressive moduli and are likely to be compressed the most upon impact.<sup>40</sup> The amide III stretching mode at 1268 cm<sup>-1</sup> in collagen fibers is considered to vibrate along a direction perpendicular to the long axis of collagen fibril.<sup>12</sup> A red shift in our parallel polarized amide III Raman bands found after impact suggests a compression of the amide III vibration.<sup>11</sup> A small split in the amide III band was also observed in the perpendicular polarized Raman band, indicating that the polarized Raman signals arises from the impacted in-plane amide III carbonyl groups in both the superficial and deep layers of cartilage. Since the collagen fibers in these regions are oriented perpendicular to each other,<sup>9,19,20</sup> the carbonyl groups are likewise oriented approximately perpendicular to each other.<sup>40</sup> Hence, the external compression approximately parallel and perpendicular to the bond direction may have likely led to the in-plane carbonyl bond experiencing both tensile and compressive loadings. This results in a blue and red shift of the amide III Raman band of

the cartilage explants, such that the amide III doublet is generated after impact. Nonetheless, further Raman spectroscopy studies are still required to better understand the relationship between the amide III polarized Raman shifts and compression on perpendicularly oriented collagen fibres.

Our parallel polarized Raman spectra also detected<sup>10,29,41</sup> GAG-associated Raman bands of cartilage appearing at 1042, 1063, 1126, 1160, and 1554 cm<sup>-1</sup>. Varying exposure times for each Raman spectra and possible varying GAG concentrations at different cartilage locations may have resulted in the varying significance of the GAG contribution to the Raman spectra.<sup>13,30</sup> Despite previous studies suggesting that GAG possesses neither intrinsic nor form birefringence except under the influence of certain dyes,<sup>42,43</sup> our polarized Raman spectra [arrows in Figs. 4(b) and 4(c)] revealed a distinct parallel dichroism in the GAG-associated pyranose band at 1042 cm<sup>-1</sup> that may be useful for characterizing structural changes of cartilage in tissue. A loss of GAG orientation was previously shown to be a possible indicator of osteoarthritis.<sup>42</sup> However, to more adequately characterize the possible orientation changes of GAG using this band, there we must obtain polarized Raman data from

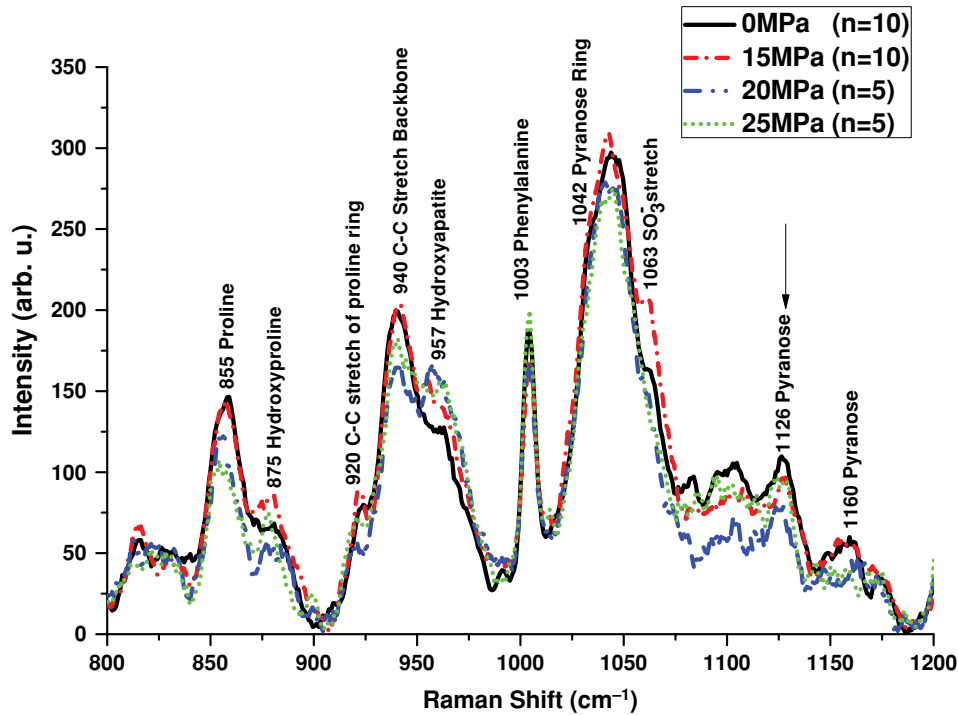


**Fig. 5** Comparison of mean parallel polarized Raman spectra in the region of 800 to 1200  $\text{cm}^{-1}$  among the control and impacted porcine cartilage explants at 15, 20, and 25 Mpa, respectively, obtained 7 days after impact. The single arrow indicates the pyranose ring group, where a significant decrease in intensity is observed after impact [see Fig. 1(c)].

cartilage with GAG chains in a known orientation. Nonetheless, the pyranose band at 1126  $\text{cm}^{-1}$  reflected a significant decrease in intensity for mildly and severely disrupted cartilage. This is consistent with the histology slides (Fig. 3), which show an ob-

servable decrease in the proteoglycans staining for all impacted groups, suggesting the possible decrease in the GAG content which is the hallmark of early osteoarthritis.<sup>16-18</sup> The sulfate band at 1063  $\text{cm}^{-1}$  associated with chondroitin sulfate<sup>10</sup> (GAG) was only detected in the mildly disrupted cartilage (15-MPa impact group) (Fig. 5). Compared to the nonpolarized pyranose Raman band at 1126  $\text{cm}^{-1}$  [Fig. 6(a)], the use of polarized Raman spectroscopy provides a more sensitive detection of changes of the GAG compositions in cartilage.

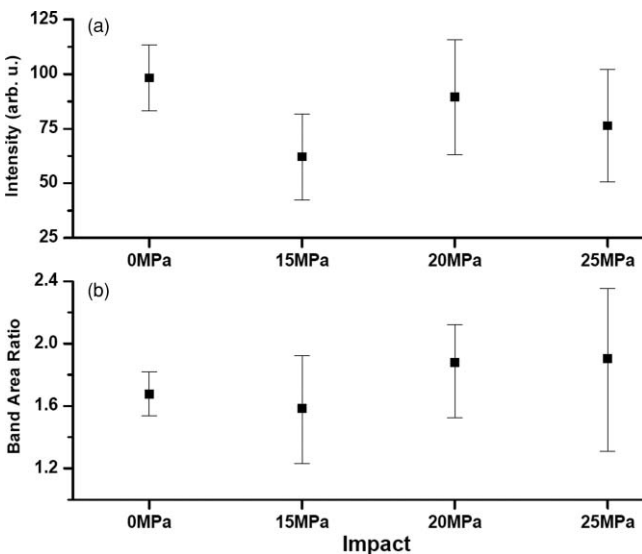


**Fig. 6** (a) Comparison of mean nonpolarized pyranose Raman band intensity at 1126  $\text{cm}^{-1}$  among control and impacted porcine explants, note that each impact group is not statistically different from the control group ( $p = 1$ ); and (b) comparison of mean nonpolarized band area ratio of proline (856  $\text{cm}^{-1}$ ) to hydroxyproline (875  $\text{cm}^{-1}$ ) among control and impacted cartilage explants, where each impact group is not statistically different from the control group ( $p = 1$ ). The y axis error bars indicate  $\pm 1$  SD.

**Table 3** Comparison of the Raman shift and the  $p$  value (one-way ANOVA with *post hoc* Bonferroni test) of the amide III peak positions obtained from the parallel polarized Raman spectra for control and impacted cartilage explants.

Groups	Raman Shift of the Amide III Bband ( $\text{cm}^{-1}$ )	
	Nonpolarized	Parallel Polarized
0 MPa (control) (n = 10)	1265.6 $\pm$ 2.5	1263.9 $\pm$ 2.1
15 MPa (n = 10)	1269.3 $\pm$ 1.3 (s) ( $p = 0.0054$ )	1266.7 $\pm$ 3.7 (s) ( $p = 0.042$ )
20 MPa (n = 5)	1269.8 $\pm$ 1.8 (s) ( $p = 0.0099$ )	1269 $\pm$ 3.4 (s) ( $p = 0.019$ )
25 MPa (n = 5)	1270.4 $\pm$ 2.1 (s) ( $p = 0.0025$ )	1269.8 $\pm$ 3.9 (s) ( $p = 0.0027$ )

n = number of explants.  
s = significant difference compared to control group,  $p < 0.05$ .

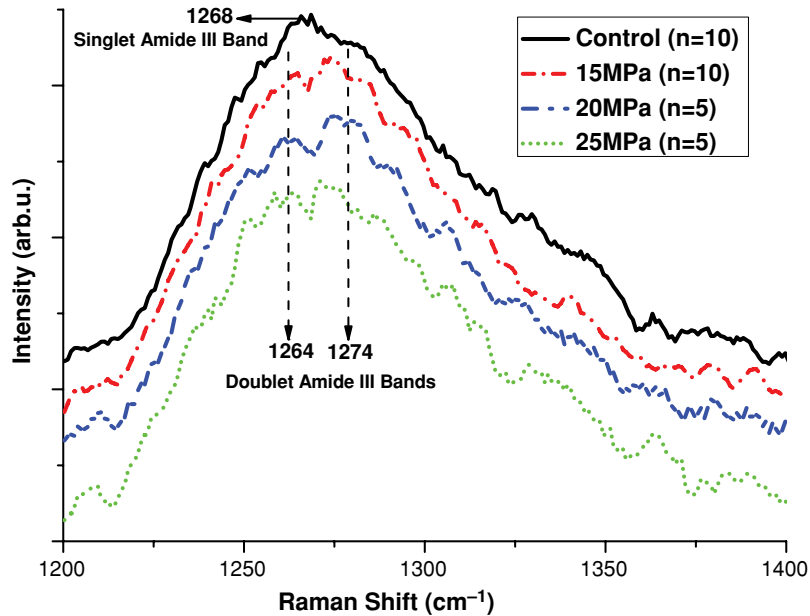


**Fig. 7** Comparison of the mean perpendicular polarized Raman spectra from 800 to 1200  $\text{cm}^{-1}$  among control and impact groups. The singlet amide III Raman peak at 1268  $\text{cm}^{-1}$  is observed for the control group, while the doublet amide III peaks at 1264 and 1274  $\text{cm}^{-1}$  are found for all impact groups. The amide III Raman bands have been vertically shifted for better visualization.

## 5 Conclusions

We demonstrated the feasibility of polarized Raman spectroscopy to effectively detect a wide spectrum of biomolecular changes associated with cartilage damage prior to visible histological changes. A significant decrease in parallel polarized pyranose ring Raman band at 1126  $\text{cm}^{-1}$  suggests a decrease in the GAG content in early cartilage damage even before significant structural disruptions can be found by histology or chondrocyte death by confocal fluorescence microscopy. Furthermore, amide III Raman bands, which exhibit a red Raman shift from 1264 to 1274  $\text{cm}^{-1}$ , reflect a possible compression of C—N vibration in collagen fibers. It is anticipated that with the development of miniature Raman probes coupled with a rapid-acquisition Raman system,<sup>26,44,45</sup> polarized Raman spectroscopy can be a clinically powerful tool for *in vivo* diagnosis and detection of early disrupted cartilage at the molecular level.

## Acknowledgments

This research is supported in part by the Biomedical Research Council, the National Medical Research Council, and the Faculty Research Fund from the National University of Singapore.

## References

- J. H. Dashefsky, "Arthroscopic measurement of chondromalacia of patella cartilage using a microminiature pressure transducer," *Arthroscopy J. Arthrosc. Rel. Surg.* **3**, 80–85 (1987).
- T. Franz, E. M. Hasler, R. Hagg, C. Weiler, R. P. Jakob, and P. Mainil-Varlet, "In situ compressive stiffness, biochemical composition, and structural integrity of articular cartilage of the human knee joint," *Osteoarthr. Cartil.* **9**, 582–592 (2001).
- F. Shapiro, S. Koide, and M. J. Glimcher, "Cell origin and differentiation in the repair of full-thickness defects of articular cartilage," *J. Bone Joint Surg. Am.* **75**, 532–553 (1993).
- D. Burstein and M. L. Gray, "Is MRI fulfilling its promise for molecular imaging of cartilage in arthritis?" *Osteoarthr. Cartil.* **14**, 1087–1090 (2006).
- H. A. Alhadlaq, Y. Xia, J. B. Moody, and J. R. Matyas, "Detecting structural changes in early experimental osteoarthritis of tibial cartilage by microscopic magnetic resonance imaging and polarised light microscopy," *Ann. Rheum. Dis.* **63**, 709–717 (2004).
- P. Mansfield and P. Glover, "Limits to magnetic resonance microscopy," *Rep. Prog. Phys.* **65**, 1489–1511 (2002).
- S. Gamsjager, M. Kazanci, E. Paschalis, P. Fratzl, Y. K. Min, S. Naito, H. Yamazaki, E. Kohda, and H. Hamaguchi, "Medical applications," Chaps. 9 and 10 in *Raman Spectroscopy for Soft Matter Applications*, M. S. Amer, Ed., pp. 225–301, Wiley-Blackwell, Hoboken, NJ (2009).
- D. Chenery and H. Bowering, "Infrared and Raman spectroscopic imaging in biosciences," *Spectrosc. Eur.* **14**, 8–14 (2003).
- V. C. Mow, W. Y. Gu, and F. H. Chen, "Structure and function of articular cartilage and menisci," Chap. 5 in *Basic Orthopaedic Biomechanics and Mechano-Biology*, V. C. Mow and R. Huiskes, Eds., pp. 181–258, Lippincott Williams & Wilkins, Philadelphia (2005).
- R. Ellis, E. Green, and C. P. Winlove, "Structural analysis of glycosaminoglycans and proteoglycans by means of Raman microspectrometry," *Connect. Tissue Res.* **50**, 29–36 (2009).
- Y. N. Wang, C. Galiotis, and D. L. Bader, "Determination of molecular changes in soft tissues under strain using laser Raman microscopy," *J. Biomech.* **33**, 483–486 (2000).
- A. Bonifacio and V. Sergo, "Effects of sample orientation in Raman microspectroscopy of collagen fibers and their impact on the interpretation of the amide III band," *Vibrat. Spectrosc.* **53**, 314–317 (2010).
- K. A. Dehring, A. R. Smukler, B. J. Roessler, and M. D. Morris, "Correlating changes in collagen secondary structure with aging and defective type II collagen by Raman spectroscopy," *Appl. Spectrosc.* **60**, 366–372 (2006).
- K. A. Dehring, N. J. Crane, A. R. Smukler, J. B. McHugh, B. J. Roessler, and M. D. Morris, "Identifying chemical changes in subchondral bone taken from murine knee joints using Raman spectroscopy," *Appl. Spectrosc.* **60**, 1134–1141 (2006).
- M. Kazanci, P. Roschger, E. P. Paschalis, K. Klaushofer, and P. Fratzl, "Bone osteonal tissues by Raman spectral mapping: orientation-composition," *J. Struct. Biol.* **156**, 489–496 (2006).

16. C. H. Yeow, S. T. Lau, P. V. S. Lee, and J. C. H. Goh, "Damage and degenerative changes in menisci-covered and exposed tibial osteochondral regions after simulated landing impact compression—a porcine study," *J. Orthop. Res.* **27**, 1100–1108 (2009).
17. B. J. Ewers, D. Dvoracek-Driksna, M. W. Orth, and R. C. Haut, "The extent of matrix damage and chondrocyte death in mechanically traumatized articular cartilage explants depends on rate of loading," *J. Orthop. Res.* **19**, 779–784 (2001).
18. P. A. Torzilli, R. Grigiene, J. Borrelli, and D. L. Helfet, "Effect of impact load on articular cartilage: cell metabolism and viability, and matrix water content," *J. Biomech. Eng.* **121**, 433–441 (1999).
19. M. T. Bayliss, M. Venn, A. Maroudas, and S. Y. Ali, "Structure of proteoglycans from different layers of human articular cartilage," *Biochem. J.* **209**, 387–400 (1983).
20. A. Maroudas, M. T. Bayliss, and M. F. Venn, "Further studies on the composition of human femoral head cartilage," *Ann. Rheum. Dis.* **39**, 514–523 (1980).
21. T. M. Quinn, P. Dierickx, and A. J. Grodzinsky, "Glycosaminoglycan network geometry may contribute to anisotropic hydraulic permeability in cartilage under compression," *J. Biomech.* **34**, 1483–1490 (2001).
22. H. J. Mankin and L. Lippiello, "Biochemical and metabolic abnormalities in articular cartilage from osteo-arthritic human hips," *J. Bone Joint Surg. Am.* **52**, 424–434 (1970).
23. T. Xie, S. Guo, J. Zhang, Z. Chen, and G. M. Peavy, "Determination of characteristics of degenerative joint disease using optical coherence tomography and polarization sensitive optical coherence tomography," *Lasers Surg. Med.* **38**, 852–865 (2006).
24. R. U. Kleemann, D. Krockner, A. Cedraró, J. Tuischer, and G. N. Duda, "Altered cartilage mechanics and histology in knee osteoarthritis: relation to clinical assessment (ICRS Grade)," *Osteoarthr. Cartil.* **13**, 958–963 (2005).
25. C. Yuen, W. Zheng, and Z. Huang, "Improving surface-enhanced Raman scattering effect using gold-coated hierarchical polystyrene bead substrates modified with postgrowth microwave treatment," *J. Biomed. Opt.* **13**(6), 064040 (2008).
26. Z. Huang, H. Zeng, I. Hamzavi, D. I. McLean, and H. Lui, "A rapid near-infrared Raman spectroscopic system for real-time *in vivo* skin measurements," *Opt. Lett.* **26**, 1782–1784 (2001).
27. Z. Huang, A. McWilliams, H. Lui, D. I. McLean, S. Lam, and H. Zeng, "Near-infrared Raman spectroscopy for optical diagnosis of lung cancer," *Int. J. Cancer* **107**, 1047–1052 (2003).
28. M. N. Leger and A. G. Ryder, "Comparison of derivative preprocessing and automated polynomial baseline correction method for classification and quantification of narcotics in solid mixtures," *Appl. Spectrosc.* **60**, 182–193 (2006).
29. Z. Huang, H. Lin, X. K. Chen, D. McLean, and H. Zeng, "Raman spectroscopy of *in vivo* cutaneous melanin," *J. Biomed. Opt.* **9**, 1198–1205 (2004).
30. N. Ignatieva, O. Zakharkina, G. Leroy, E. Sobol, N. Vorobieva, and S. Mordon, "Molecular processes and structural alterations in laser reshaping of cartilage," *Laser Phys. Lett.* **4**, 749–753 (2007).
31. C. A. M. Huser and M. E. Davies, "Validation of an *in vitro* single-impact load model of the initiation of osteoarthritis-like changes in articular cartilage," *J. Orthop. Res.* **24**, 725–732 (2006).
32. A. Lahm, M. Uhl, C. Ergelet, J. Haberstroh, and E. Mrosek, "Articular cartilage degeneration after acute subchondral bone damage: an experimental study in dogs with histopathological grading," *Acta Orthop. Scand.* **75**, 762–767 (2004).
33. K. A. Lozoya and J. B. Flores, "A novel rat osteoarthritis model to assess apoptosis and matrix degradation," *Pathol. Res. Pract.* **196**, 729–745 (2000).
34. G. Penel, C. Delfosse, M. Descamps, and G. Leroy, "Composition of bone and apatitic biomaterials as revealed by intravital Raman microspectroscopy," *Bone* **36**, 893–901 (2005).
35. J. Engel and H. P. Baechinger, "Structure stability and folding of collagen triple helix," Chap. 2 in *Topics in Current Chemistry: Collagen Primer in Structure, Processing and Assembly*, D. E. Birk and P. Bruckner, Eds., pp. 7–33, Springer-Verlag Berlin Heidelberg, Netherlands (2005).
36. M. Chvapil and V. Kobrle, "Changes in proline and hydroxyproline in collagens during the development of rats," *Experientia* **XVII**, 226–227 (1960).
37. A. M. Gil, E. Buñuel, P. López, and C. Cativiela, "Synthesis of enantiopure 7-azanorbornane proline- $\alpha$ -amino acid chimeras by highly efficient HPLC resolution of a phenylalanine analogue," *Tetrahed. Asymm.* **15**, 811–819 (2004).
38. L. Lippiello, D. Hall, and H. J. Mankin, "Collagen synthesis in normal and osteoarthritic cartilage," *J. Clin. Invest.* **59**, 593–600 (1977).
39. R. U. Repo and J. B. Finlay, "Survival of articular cartilage after controlled impact," *J. Bone Joint Surg. Am.* **59**, 1068–1076 (1977).
40. Y. Xia, H. Alhadlaq, N. Ramakrishnan, A. Bidthanapally, F. Badar, and M. Lu, "Molecular and morphological adaptations in compressed articular cartilage by polarized light microscopy and Fourier-transform infrared imaging," *J. Struct. Biol.* **164**, 88–95 (2008).
41. K. Potter, L. H. Kidder, I. W. Levin, E. N. Lewis, and R. G. S. Spencer, "Imaging of collagen and proteoglycan in cartilage sections using Fourier transform infrared spectral imaging," *Arthritis. Rheum.* **44**, 846–855 (2001).
42. J. Dunham, D. R. Shackleton, A. M. Nahir, M. E. J. Billingham, L. B. Chayen, and I. H. Muir, "Altered orientation of glycosaminoglycans and cellular changes in the tibial cartilage in the first two weeks of experimental canine osteoarthritis," *J. Orthop. Res.* **3**, 258–268 (2005).
43. J. Dunham, M. G. Chambers, M. K. Jasani, L. Bitensky, and J. Chayen, "Changes in the orientation of proteoglycans during the early development of natural murine osteoarthritis," *J. Orthop. Res.* **8**, 101–104 (2005).
44. Z. Huang, S. Teh, W. Zheng, J. Mo, K. Lin, X. Shao, K. Ho, M. Teh, and K. Yeoh, "Integrated Raman spectroscopy and trimodal wide-field imaging techniques for real-time *in vivo* tissue Raman measurements at endoscopy," *Opt. Lett.* **34**, 758–760 (2009).
45. Z. Huang, M. Bergholt, W. Zheng, K. Lin, K. Ho, M. Teh, and K. Yeoh, "In vivo early diagnosis of gastric dysplasia using narrow-band image-guided Raman endoscopy," *J. Biomed. Opt.* **15**, 037017 (2010).